61

NUMERICAL INVESTIGATION ON BEHAVIOR OF 2D FLOOD FLOWS AND HYDRODYNAMIC FORCES EXERTING ON STRUCTURES

By

Mirei SHIGE-EDA, Juichiro AKIYAMA

Department of Civil Engineering, Kyushu Institute of Technology
Sensuicho 1-1, Tobata, Kitakyushu 804-8550, JAPAN

Masaru URA

Hinosato 9-5-5, Munakata 811-3425, JAPAN

and

Toshihiko KOBAYASHI

Okumura Corporation
Matuzakicho 2-2-2, Abeno, Osaka 545-8555, JAPAN

SYNOPSIS

The behavior of 2D flood flows in flood plain with structures and the hydrodynamic forces acting on structures were investigated experimentally and numerically. Front positions, depths and surface velocities of flood flows as well as hydrodynamic forces acting on the structures were observed in experiments. Comparisons of numerical results with these experimental data demonstrated that a numerical model based on FDS technique and unstructured FVM for 2D flood flows (FUF-2DF model) can simulate the behavior of 2D flood flows as well as the forces acting on structures with reasonable accuracy. A numerical simulation of flood flows in a proto-scale urban area was also carried out to demonstrate the capability of the FUF-2DF model for predicting possible flooding scenario and for estimating the degree of structural damage.

INTRODUCTION

In recent years, flooding due to heavy rain fall in the densely populated and highly developed areas have been increasing in many parts of the world. In urban areas, the importance of the interaction between flood flows and complicated flood plain geometries with structures, road networks and so on for predicting the behavior of flood flows and risk analysis for structural failure has been recognized ((10),(14)). Numerical models are useful in investigating and predicting possible flooding scenario, which can then be used to formulate suitable flood hazard mitigation measures.

Several models for simulating 2D flood flows have been reported in recent years ((3), (4), (5), (6), (8), (13), (15), (16)). Some models((3), (5), (8)) have been verified against experimental data on flood flow on featureless horizontal or sloping bed. For extensive verifications of the model, reliable experimental data on both flow depths and velocities of flows in complicated flood domain, need to be compared with computed results. However,
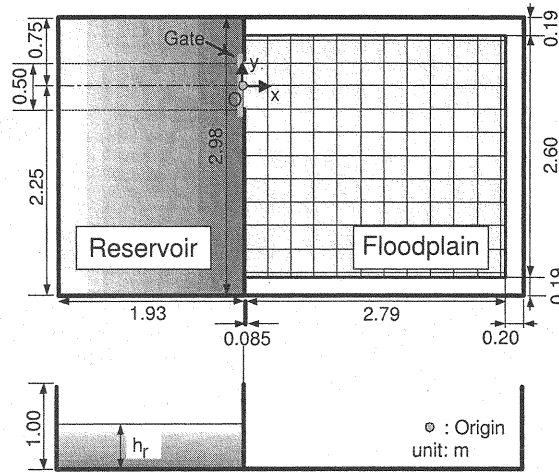
Fig.1 Experimental Set-ups

as far as we know, the quantitative verifications on flow depth and velocities in flood plain with structures have not been reported since there has been no experimental data on flow velocities.

The degree of structural damage is related to the hydrodynamic forces acting on a structure (10). Fukuoka et al. (7) studied the forces on the square shape structure in uniform flows, and showed that the forces acting on a structure could be computed by taking the difference of hydrostatic pressures between the front and back of the structure. Akiyama et al. (1) also showed that the relationship between hydrodynamic force and hydrostatic pressure described above could be applied even when the angle of attack of a square pillar was changed. Ramsden and Raichlen (11) showed that the observed forces on a vertical wall due to bores and the computed forces assuming the hydrostatic pressure distribution agreed reasonably well, except for a brief time after the bore front reached the wall.
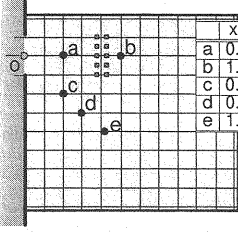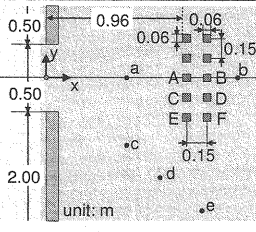
In this paper, the behavior of 2D flood flows in flood plain with structures and the hydrodynamic forces acting on structures are investigated experimentally and numerically. In the experiments, front positions, depths and surface velocities of flood flows as well as forces acting on structures were quantified. The accuracy and applicability of the FUF-2DF model (a numerical model based on Flux-Difference Splitting (FDS)(12) technique and Unstructured Finite-volume method (FVM) for 2D Flood flows) were verified against these experimental data. In addition, a numerical simulation of flood flows in a proto-scale urban area was performed.

EXPERIMENTS

The experimental set-ups consist of a reservoir and a flood plain separated by a gate-fitted wall as shown in Fig.1. The reservoir is 1.93m long and 3.0m wide, while the flood plain is 2.79m long and 2.6m wide. The beds of both the reservoir and flood plain are horizontal and made of acrylic boards. The flood plain has open boundaries on all sides. The gate is 0.5m wide and located at 0.75m from the left-side end of the wall separating the reservoir from the flood plain.

The experimental conditions are shown in Table 1. Structures such as houses and

Table1 Experimental Conditions

Initial Depth in Reservoir h_r (m)	Locations of Observation Stations	Arrangement of Square Pillars
0.2		

Locations of Observation Stations:

	x (m)	y (m)
a	0.585	0.00
b	1.335	0.00
c	0.585	-0.50
d	0.835	-0.75
e	1.135	-1.00

Fig.2 Example of Dam-break Flows with Structures

buildings were modeled by placing 0.06m wide and 0.2m tall square pillars in flood plain. These pillars are tall enough to be unsubmerged. The reservoir had an initial depth h_r, while the flood plain was initially dry. The dam-break flows were simulated by instantaneously opening the gate separating the reservoir and the flood plain. An example of the dam-break flows is shown in Fig.2.

The flood wave front positions, flow depths and surface velocities at each observation station (Table 1) were observed. The hydrodynamic forces acting on structures $A \sim F$ (Table 1) were also observed. Flood wave front position was visualized and recorded with a digital VTR, and analyzed by a computer. Flow depths were determined by analyzing the water surface profiles, which were visualized by a laser light sheet and recorded with a digital VTR. Surface velocities U_s were obtained by analyzing the motion of foam polystyrene particles with diameter = 6 mm, floating on the water surface, with Particle Tracking Velocimetry (PTV). From measurements of U_s, the depth-averaged velocities U_a were calculated as $U_a = 0.90U_s$. This relationship was obtained by means of the logarithmic law, and was verified in the case of 1D dam-break flow by Akiyama et al.(2). The hydrodynamic forces acting on the structures were determined by a 2-component load cell. Each experiment was repeated at least 4 times under the same conditions in order to improve data reliability.

FUF-2DF MODEL

Since the FUF-2DF model is the same as the reference (3), the outline of the model is shown briefly here. The FUF-2DF model(3) uses the following 2D shallow water equation

as the governing equation

$$\frac{\partial \boldsymbol{U}}{\partial t} + \frac{\partial \boldsymbol{E}}{\partial x} + \frac{\partial \boldsymbol{F}}{\partial y} + \boldsymbol{S} = \boldsymbol{0} \tag{1}$$

where $\boldsymbol{U}$ = flow vector; $\boldsymbol{E}$ and $\boldsymbol{F}$ = flux vectors; $\boldsymbol{S}$ = vector containing source and sink terms. The above vectors are given by

$$\boldsymbol{U} = \begin{pmatrix} h \\ uh \\ vh \end{pmatrix} ; \boldsymbol{E} = \begin{pmatrix} uh \\ u^2h + \frac{1}{2}gh^2 \\ uvh \end{pmatrix} ;$$

$$\boldsymbol{F} = \begin{pmatrix} vh \\ uvh \\ v^2h + \frac{1}{2}gh^2 \end{pmatrix} ; \boldsymbol{S} = \begin{pmatrix} 0 \\ -gh\left(S_{ox} - S_{fx}\right) \\ -gh\left(S_{oy} - S_{fy}\right) \end{pmatrix} \tag{2}$$

where h = flow depth; u, v = flow velocities along x- and y-direction, respectively; g = acceleration due to gravity; S_{ox} and S_{oy} = bed slopes along x- and y-direction = $-\partial z_b/\partial x$ and $-\partial z_b/\partial y$, respectively; z_b = bed elevation; S_{fx} and S_{fy} = friction slopes along x- and y-direction, respectively. The friction slopes are estimated as

$$S_{fx} = \frac{n^2 u \sqrt{u^2 + v^2}}{h^{4/3}} \quad ; \quad S_{fy} = \frac{n^2 v \sqrt{u^2 + v^2}}{h^{4/3}} \tag{3}$$

where n = Manning's roughness coefficient.

The flux vectors $\boldsymbol{E}$ and $\boldsymbol{F}$ are related to $\boldsymbol{U}$ through their Jacobian matrices $\boldsymbol{A}$ and $\boldsymbol{B}$ as

$$\boldsymbol{A} = \frac{\partial \boldsymbol{E}}{\partial \boldsymbol{U}} = \begin{pmatrix} 0 & 1 & 0 \\ -u^2 + c^2 & 2u & 0 \\ -uv & v & u \end{pmatrix} ; \boldsymbol{B} = \frac{\partial \boldsymbol{F}}{\partial \boldsymbol{U}} = \begin{pmatrix} 0 & 0 & 1 \\ -uv & v & u \\ -v^2 + c^2 & 0 & 2v \end{pmatrix} \tag{4}$$

where c = celerity= $\sqrt{gh}$.

The integral form of the governing equations is obtained by integrating Eq.1 over a control volume Ω using the Gauss divergence theorem as

$$\frac{\partial}{\partial t} \int_{\Omega} \boldsymbol{U} dS + \oint_{\partial \Omega} (\boldsymbol{\mathcal{F}} \cdot \boldsymbol{n}) dL + \int_{\Omega} \boldsymbol{S} dS = \boldsymbol{0} \tag{5}$$

where $\boldsymbol{n}$ = outward-pointing unit vector normal to the cell face $\partial\Omega = (n_x, n_y)$; $\boldsymbol{\mathcal{F}} \cdot \boldsymbol{n} = \boldsymbol{E}n_x + \boldsymbol{F}n_y$ is normal flux vector; dL = length of $\partial\Omega$, dS = area of Ω.

The normal flux vector $\boldsymbol{\mathcal{F}} \cdot \boldsymbol{n}$ is related to $\boldsymbol{U}$ through its Jacobian matrix $\boldsymbol{C_n}$ as

$$\boldsymbol{C}_n = \frac{\partial (\boldsymbol{\mathcal{F}} \cdot \boldsymbol{n})}{\partial \boldsymbol{U}} = \boldsymbol{A}n_x + \boldsymbol{B}n_y \tag{6}$$

Eq.5 is numerically integrated by using the unstructured finite volume discretisation and a forward Euler time discretisation. Also, the numerical flux through the cell faces is calculated by FDS technique (12).

The FUF-2DF model uses an unstructured grid system. In the system, grid sizes may be varied in computational domain to fit the local geometry, enabling the laying out of the grid around complicated geometries to be easier and more correct than a structured grid system. Considering the ability of the grid system, the FUF-2DF model is thought to have the capability of reproducing complicated urban area with structures, road networks etc.
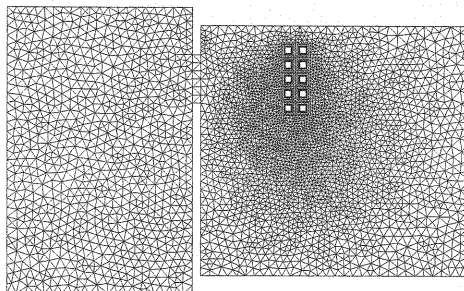
Fig.3 Grid layout

MODEL VERIFICATION

Numerical experiments on 1D dam-break flows confirm that the FUF-2DF model always yields stable results if the flood plain tail water depth remains above $h_v=0.00001$m. In the computations, the minimum depth in a flood plain was initially set to $h_v=0.00001$m. The bed friction term computed by Eq.3 may become unrealistically high when the depth remains below 0.001m. In such cases, the bed friction was set to zero. Manning's roughness coefficient was set to 0.01 for the acrylic bed. The computational area was divided into 7965 cells as shown in Fig.3.

Fig.4 compares the computed front positions with the observed data at different times. In the computations, the interface between the depths h and h_v was defined as the front position. It can be seen that the overall agreement between computed front positions and observed ones is satisfactory although the predicted front propagation speed along the centerline of the gate is slightly slower than the observed one.

Figs.5 and 6 compare the computed depths and velocities with the observed data at each observation station, respectively. It was observed that the flow depths and velocities rose suddenly in the beginning. The sudden rise of depths and velocities indicated the arrival of the flood wave front. At Station a, near the gate, for the initial several seconds after opening of the gate, the computed depths were lower than the observed data. Thereafter, although the computed depths are slightly higher than the observed data, the agreement between the computed and observed data was generally satisfactory (Fig.5 (a)). At Station b, behind the structures, it was observed that the flow was strongly affected by the structures, so that the flow changed rapidly and became irregular. Under the flow phenomena, the assumption is that hydrostatic pressure and negligible effective stress is seriously compromised, and this is reflected in the discrepancy between the computed and observed flood depths. In the initial several seconds after opening of the gate, the computed depths are lower than the observed data. As time passes, the discrepancy between computed and observed depths decreases (Fig.5 (b)). At Station c, although the computed depths are slightly higher than the observed data, the agreement between the computed and observed data is generally satisfactory (Fig.5 (c)). At Station d, which is away from the gate center axis, the computed depths mostly agree with the observed data (Fig.5 (d)). At Station e, the flow depth shows a rapid rise initially followed by a slight drop and a second rapid rise before beginning to decrease gradually (Fig.5 (e)). The presence of structures complicates the flow and produces such variations in depth. The computed depths reproduce the trend although some discrepancy in the magnitude is noted. At Stations a and $c{\sim}e$, the agreement between computed velocities and observed data is generally satisfactory (Figs.6 (a)${\sim}$(d)).

(a) t=1.25 (s)　　　　(b) t=1.50 (s)　　　　(c) t=1.75 (s)
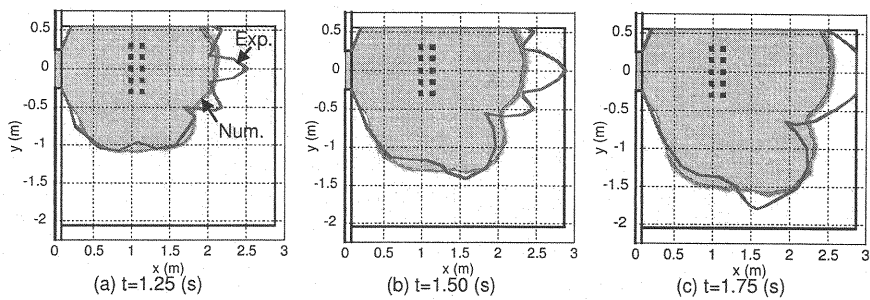
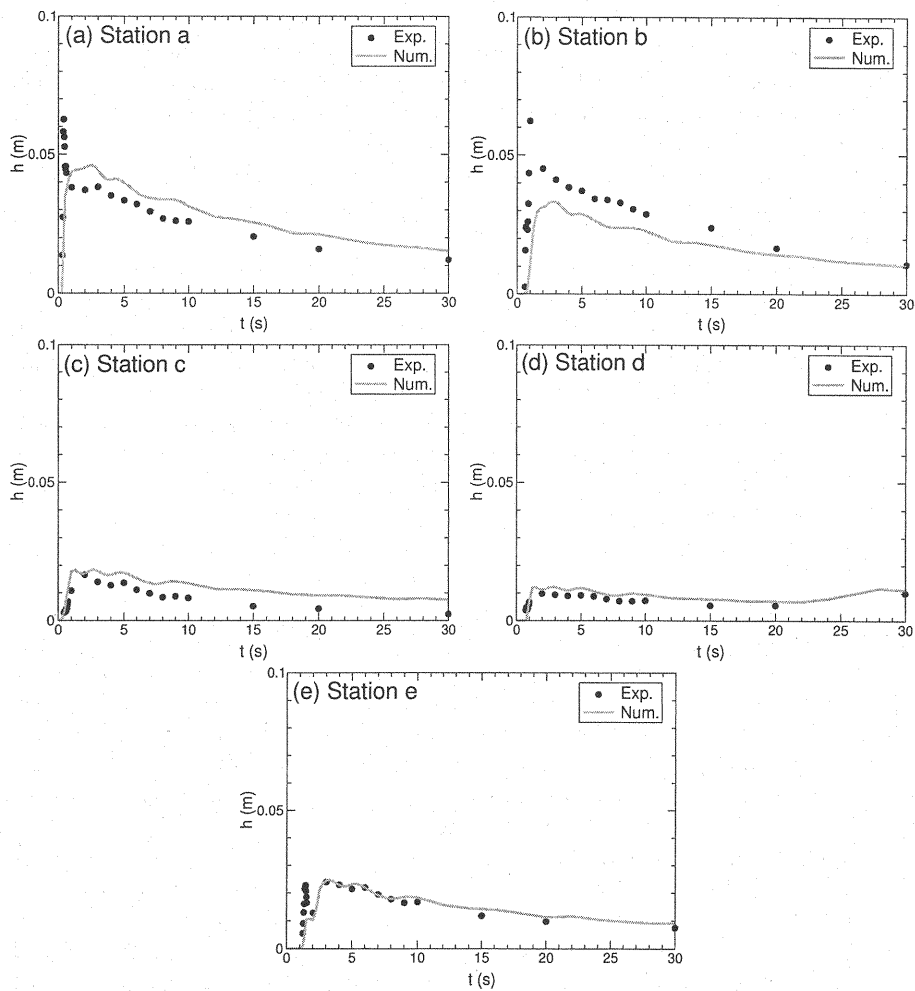**Fig.4** Comparison of Computed and Observed Front positions

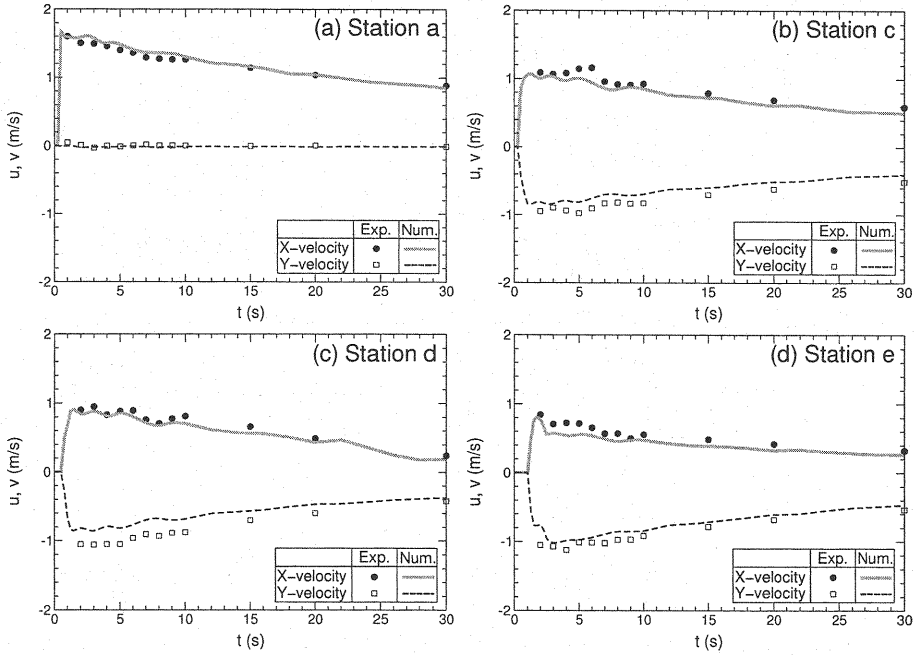**Fig.5** Comparison of Computed and Observed Depths

Fig.6 Comparison of Computed and Observed Velocities

The above findings demonstrate that as long as the flow conforms to the assumption underlying the governing equations, the FUF-2DF model can largely predict the depths and velocities of 2D flood flows on a horizontal dry-bed with structures.

HYDRODYNAMIC FORCES ACTING ON STRUCTURES

The hydrodynamic forces acting on structures Ω', which is set to the control volume Ω in Eq.5, in the x-direction D_x and the y-direction D_y can be computed as

$$D_x = -\rho \oint_{\partial\Omega'} \frac{1}{2}gh^2 n_x dL' \,; \; D_y = -\rho \oint_{\partial\Omega'} \frac{1}{2}gh^2 n_y dL' \tag{7}$$

where ρ = the density of the water = 1000kg/m³, $\partial\Omega'$ = boundaries of structure, L' = the length of $\partial\Omega'$.

Fig.7 compares the computed forces with observed data at Structures ($A{\sim}F$ in Table 1). Using the computed depth h, the hydrodynamic forces $\boldsymbol{D}$ acting on structures were computed by Eq.7. The observed forces D_x at all structures rise to their maximum in the beginning and then continue to decrease. Also the observed D_y increase as the structures are away from the gate center axis. This is captured correctly by the FUF-2DF model. On Structures A, C, E and F, the computed D_x are lower than the observed data for initial several seconds after opening of the gate. Thereafter, the computed forces and the observed data agree reasonably well for all the structures. The explanation for this trend can be found in the discussion on depths and velocities. The maximum computed forces underpredict the observed data. On the Structures B and D, the computed D_x and D_y are greater than the observed data for initial several seconds after opening of the gate. In the experiments, which were carried out, active air entrainment into the flow was observed
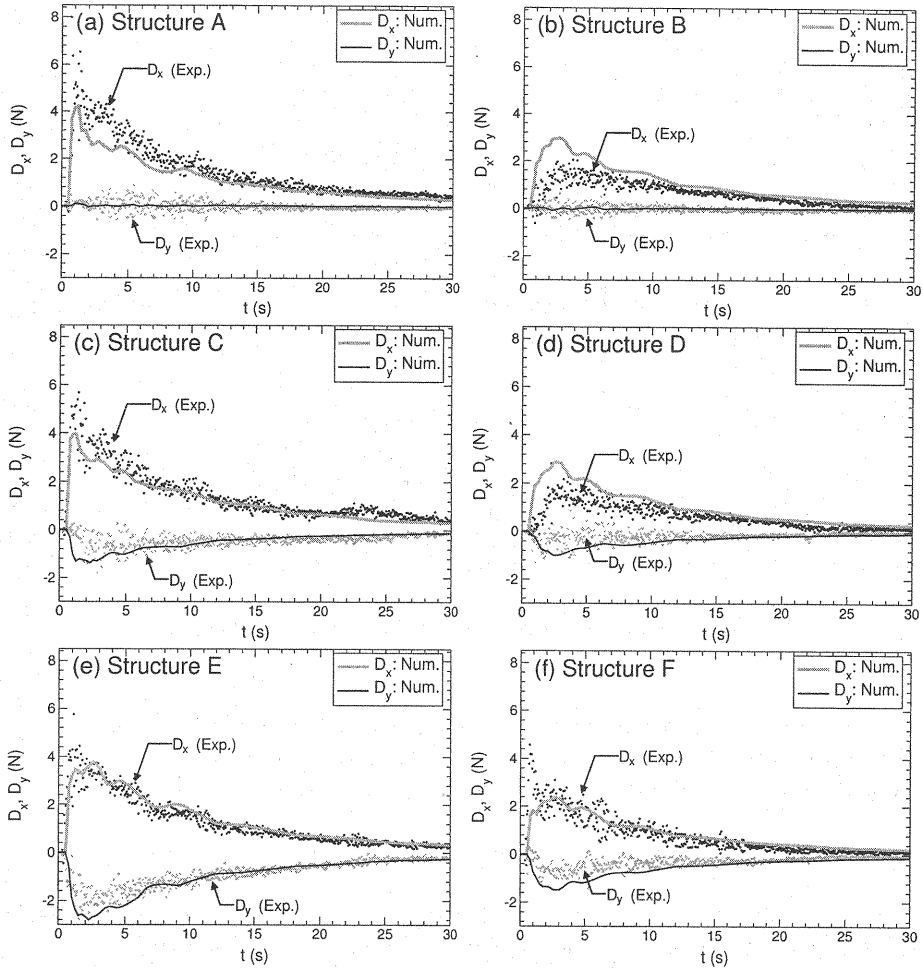
Fig.7 Comparison of Computed and Observed Forces on Structures
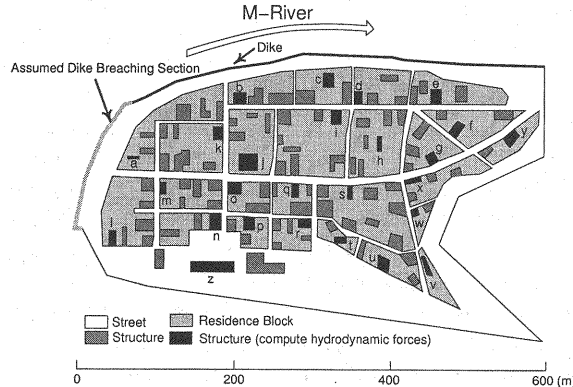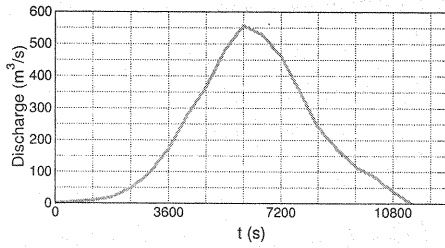

Fig.8 Model Urban Area

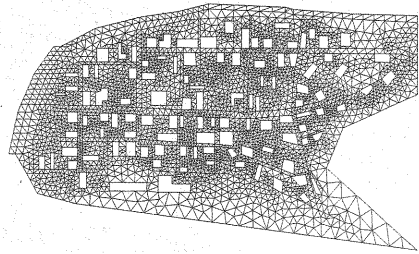Fig.9 Assumed Inundation discharge at the Dike Breaking Section

Fig.10 Grid layout in the model urban area

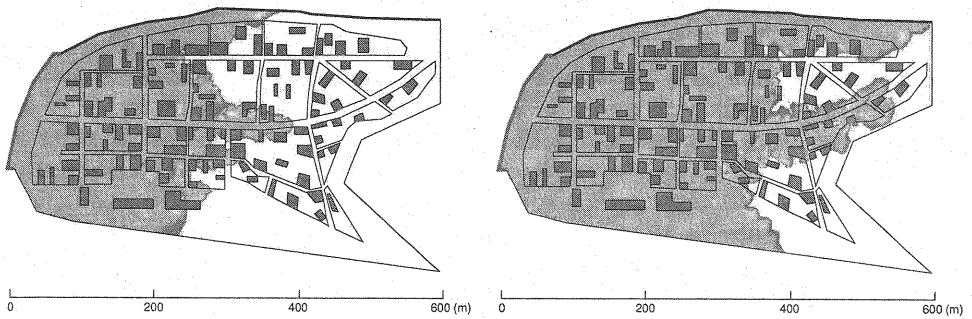

Fig.11 Computational Results of Front Positions (left: $t=$500sec, right: $t=$900sec)

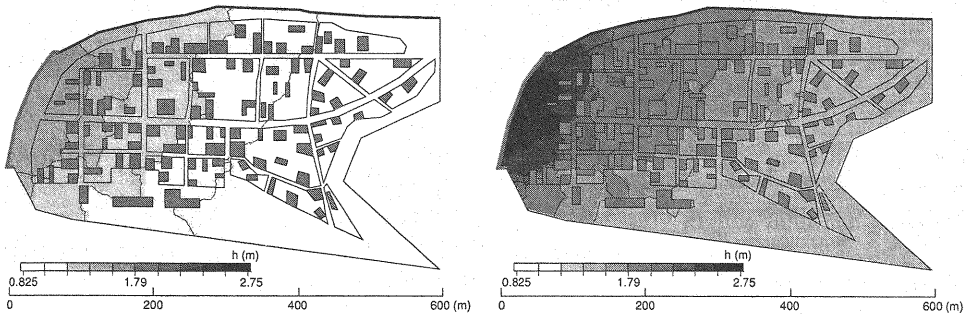
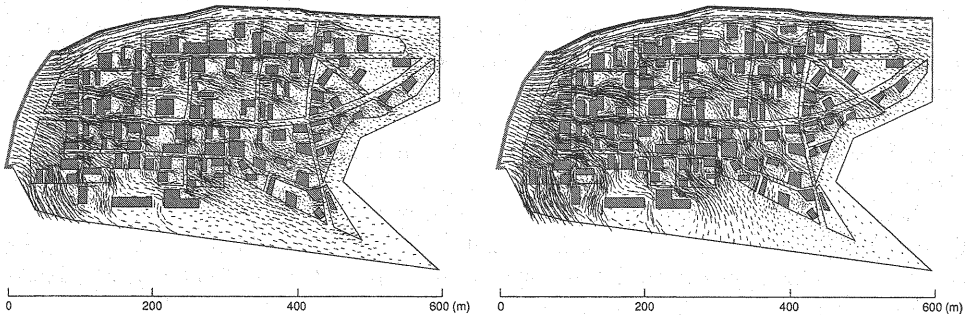Fig.12 Computational Results of Flow Depth (left: $t=$4200sec, right: $t=$6000sec)

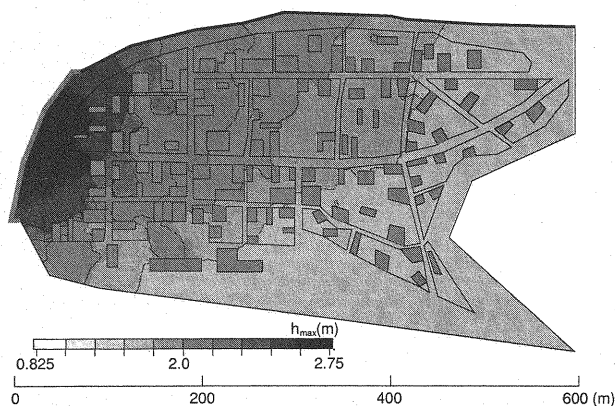Fig.13 Computational Results of Flow Velocities (left: $t=$4200sec, right: $t=$6000sec)

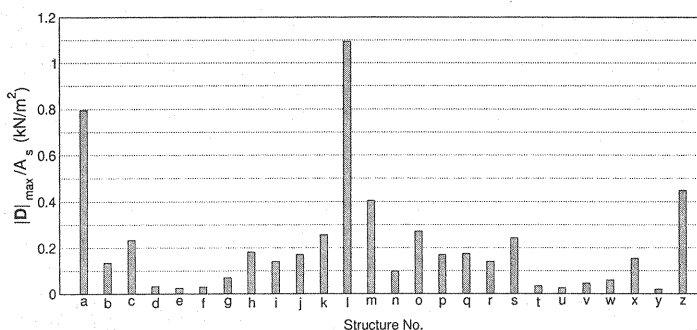**Fig.14** Computational Results of Maximum Flow Depth

Fig.15 Computational Results of a Maximum Hydrodynamic Force per Area of a Structure

during very rapid flow around the Structures B and D. Owing to this, value of density of water may have been lower than that used in the computations. As the flow became stabilized, the computed forces and the observed data agreed reasonably well.

The above findings demonstrate that the FUF-2DF model generally reproduces the observed hydrodynamic forces with reasonable accuracy.

APPLICATION OF THE MODEL TO A PROTO-SCALE URBAN AREA

The FUF-2DF model is applied to a model urban area of M-City(10), which suffered serious damage from the San-in heavy rain in July, 1983. The details of the flooding were reported in (10) and the data for the simulation such as arrangement of structures, road network was obtained easily from (10) comparatively. Fig.8 shows a model urban area of M-City. A dike breaching section and an inundation discharge at the section shown in Figs.8 and 9 were assumed according to (10), respectively. In the simulation, the bed elevations of the model area were set constant and the area was divided into 6756 computational cells as shown in Fig.10. The boundaries of a dike and structures and the boundaries of the model urban area are applied to closed boundary conditions and free out flow conditions, respectively. The values of Manning's roughness coefficients (n=0.043:street, n=0.067:residence block) are given according to (9). The value of n in residence block may be overestimated in this simulation, since the value used in (9) includes

the effects of the structures on the flows. The computational cells, which are not inundated, are applied to dry-bed conditions (3).

Figs.11, 12 and 13 show that the front positions of flood flow, flow depths and velocity vectors at different times, respectively. These figures reveal that (I) the front of flood flow tends to propagate along a wide street, and (II) a flood flow tends to accelerate between structures.

In almost all computational cells and structures, computed flow depths and hydrodynamic forces became maximum when the inundation discharge became maximum (t=6000sec (Fig.9)). Figs.14 and 15 show the computational results of maximum flow depth h_{max} and maximum hydrodynamic force $|\boldsymbol{D}|_{max}$ per unit area, respectively. This shows that (I) the maximum depth near the dike breaking section are higher than other places, and (II) the maximum hydrodynamic force per unit area of Structures a l, m and z are higher than other structures. This also indicates that the structures a, l, m and z are exposed to danger of being damaged comparing with other structures.

CONCLUSION

The behavior of two-dimensional flood flows in flood plain with structures and the hydrodynamic forces acting on the structures were investigated numerically and experimentally. The front positions, depths and surface velocities of flood flows as well as hydrodynamic forces acting on the structures were observed by using an image analysis, called PTV and a 2-component load cell, respectively. The FUF-2DF model was verified against these experimental data. It was quantitatively confirmed that the FUF-2DF model can reproduce the observed parameters with reasonable accuracy. A numerical simulation of flood flows in a proto-scale urban area was also carried out and the capability of the FUF-2DF model for estimating the degree of structureal damage was demonstrated.

ACKNOWLEDGMENT

REFERENCES

1. Akiyama, J., Shige-da, M., Kobayashi, T. and Oota, K.: Hydrodynamic force exerting on a square pillar in steady free surface shear flows, *Annual Journal of Hydraulic Engineering,* JSCE, Vol. 46, pp. 827–832, 2002, (in Japanese).

2. Akiyama, J., Shige-da, M., Kobayashi, T. and Oota, K.: Hydrodynamic force exerting on a square pillar in unsteady free surface flows, *Annual Journal of Hydraulic Engineering,* JSCE, Vol. 46, pp. 1205–1210, 2002, (in Japanese).

3. Akiyama, J., Shigeda, M. and Ura, M.: First- and second-order accurate 2D numerical model based on unstructured finite-volume method for flood flows, *Journal of Hydraulic, Coastal and Environmental Engineering,* JSCE, No. 705/II-59, pp. 31–43, 2002, (in Japanese).

4. Alcrudo, F. and Garcia-Navarro, P.: A High-resolution Godunov-type scheme in finite volumes for the 2D shallow-water equations, *International Journal Numerical Methods in Fluids,* Vol. 16, pp. 489–505, 1993.

5. Fraccarollo, L. and Toro, E. F.: Experimental and numerical assessment of the shallow water model for two-dimensional dam-break type problems, *Journal of Hydraulic Research,* Delft, The Netherlands, Vol. 33, No. 6, pp. 843–864, 1995.

6. Fujihara, M. and Borthwick, A. G. L.: Godunov-type solution of curvilinear shallow-water equations, *Journal of Hydraulic Engineering,* ASCE, Vol. 126, No. 11, pp. 827–836, 2000.

7. Fukuoka, S., Kawashima, M., Yokoyama, H. and Mizuguchi, M.: The numerical simulation model of flood induced flows in urban residential area and the study of damage reduction, *Journal of Hydraulic, Coastal and Environmental Engineering,* JSCE, No. 600/II-43, pp. 23–36, 1998, (in Japanese).

8. Jha, A. K., Akiyama, J. and Ura, M.: Flux-difference splitting schemes for 2D flood flows, *Journal of Hydraulic Engineering,* ASCE, Vol. 126, No. 1, pp. 33–42, 2000.

9. Kawaike, K., Inoue, K., Hayashi, H. and Toda, K.: Development of inundation flow model in urban area, *Journal of Hydraulic, Coastal and Environmental Engineering,* JSCE, No. 698/II-58, pp. 1–10, 2002, (in Japanese).

10. Kawata, Y. and Nakagawa, H.: Flood disasters in the Misumi river - flooding and damages of houses -, *Annuals of the Disaster Prevention Research Institute, Kyoto University,* Vol. 27B-2, pp. 1–18, 1984, (in Japanese).

11. Ramsden, J. D. and Raichlen, F.: Forces on vertical wall caused by incident bores, *Journal of Waterway, Port, Coastal, and Ocean Engineering,* ASCE, Vol. 116, No. 5, pp. 592–613, 1990.

12. Roe, P. L.: Approximate Riemann solvers, parameter vectors and difference schemes, *Journal of Computational Physics,* Vol. 43, pp. 357–372, 1981.

13. Sleigh, P. A., Gaskell, P. H., Berzins, M. and Wright, N. G.: An unstructured finite-volume algorithm for predicting flow in rivers and estuaries, *Computers & Fluids,* Vol. 27, No. 4, pp. 479–508, 1998.

14. Tachi, K., Suetugi, T., Kobayashi, H. and Tomaru, M.: Flood damage mitigation effect of groves in the floodpoain, study on the Yosasa river basin, *Annual Journal of Hydraulic Engineering,* JSCE, Vol. 45, pp. 913–918, 2001, (in Japanese).

15. Wang, J. S., Ni, H. G. and He, Y. S.: Finite-difference TVD scheme for computations of dam-break problems, *Journal of Hydraulic Engineering,* ASCE, Vol. 126, No. 4, pp. 253–262, 2000.

16. Zhao, D. H., Shen, H. W., Lai, J. S. and Tabios III, G. Q.: Approximate Riemann solvers in FVM for 2D hydraulic shock wave modeling, *Journal of Hydraulic Engineering,* ASCE, Vol. 122, No. 12, pp. 692–702, 1996.

APPENDIX-NOTATION

The following symbols are used in this paper:

U = flow vector;

E, F = flux vectors;

S = vector containing source and sink terms;

h	=	flow depth;
u, v	=	velocities along x- and y-direction, respectively;
g	=	acceleration due to gravity;
S_{ox}, S_{oy}	=	bed slopes along x- and y-direction, respectively;
S_{fx}, S_{fy}	=	friction slopes along x- and y-direction, respectively;
n	=	Manning's roughness coefficient;
c	=	celerity $(=\sqrt{gh})$;
$\boldsymbol{n}$	=	outward-pointing unit vector normal to cell face $= ((n_x, n_y))$;
$\mathcal{F} \cdot \boldsymbol{n}$	=	normal flux vector; and
$\boldsymbol{C_n}$	=	Jacobian matrix.